

Data-driven Control Design Schemes in Active Distribution Grids: Capabilities and Challenges

Stavros Karagiannopoulos^{*†}, Roel Dobbe[‡], Petros Aristidou[§], Duncan Callaway[‡], Gabriela Hug^{*}

^{*} EEH - Power Systems Laboratory, ETH Zurich, Physikstrasse 3, 8092 Zurich, Switzerland

[‡] Department of Electrical Engineering & Computer Sciences, UC Berkeley, Berkeley, USA

[§] School of Electronic and Electrical Engineering, University of Leeds, Leeds LS2 9JT, UK

Emails: {karagiannopoulos, hug}@eeh.ee.ethz.ch, {dobbe, dcal}@berkeley.edu, p.aristidou@leeds.ac.uk

Abstract—Today, system operators rely on local control of distributed energy resources (DERs), such as photovoltaic units, wind turbines and batteries, to increase operational flexibility. These schemes offer a communication-free, robust, cheap, but rather sub-optimal solution and do not fully exploit the DER capabilities. The operational flexibility of active distribution networks can be greatly enhanced by the optimal control of DERs. However, it usually requires remote monitoring and communication infrastructure, which current distribution networks lack due to the high cost and complexity. In this paper, we investigate data-driven control algorithms that use historical data, advanced off-line optimization techniques, and machine learning methods, to design local controls that emulate the optimal behavior without the use of any communication. We elaborate on the suitability of various schemes based on different local features, we investigate safety challenges arising from data-driven control schemes, and we show the performance of the optimized local controls on a three-phase, unbalanced, low-voltage, distribution network.

Index Terms—optimal control, data-driven control design, active distribution networks, OPF, machine learning

I. INTRODUCTION

Distribution systems are undergoing a tremendous transformation due to the introduction of large shares of Distributed Generators (DGs), mainly renewables. Although DGs bring some uncertainties in distribution grids, they can provide significant operational flexibility, amplifying the role of Distribution Networks (DNs) [1]. Their ability is further enhanced when combined with other Distributed Energy Resources (DERs), such as batteries and flexible loads.

The control of DERs is vital to ensure a secure, reliable and cost-effective DN operation. A first option is centralized schemes that require monitoring and communication infrastructure and usually rely on optimization methods. These schemes have become popular due to theoretical developments in the nonlinear AC power flow [2] and advances in computational power that allow for the real-time solution of such problems. Several researchers have proposed system-wide optimal operation methods by coordinated control of DERs, e.g. [3], [4]. Another option is local control schemes, e.g. [5], that rely only on local information to modify the DER behavior. They are simple, robust, communication-free and are already embedded in several grid codes. However, these methods usually employ a one-size-fits-all approach, where the same control parameters are employed in all DNs and types of DERs. Finally, distributed approaches, e.g. [6], use limited

communication between different DERs to coordinate them and achieve a close-to-optimal operation.

In this paper, we investigate data-driven control design methods that have gained a lot of attention lately. Such methods are hybrid as the controllers are "trained" using offline centralized approaches, but the derived local controls can be used when no communication infrastructure is available [7], [7]–[12]. Reference [7] uses non-linear control policies to derive reactive power injections of the inverter-based DGs, while in [8], multiple linear regression is used in an open-loop fashion to calculate a function for each inverter that maps its local historical data to pre-calculated optimal reactive power injections. However, in both works only reactive power control is considered, neglecting possible combinations with other available controls, and a balanced operation is assumed. Reference [9] considered reactive control and active power curtailment, while [10], [12] extended the available measures to controllable loads and storage systems. Furthermore, while [8], [11] design local, open-loop controllers, [9], [10], [12] employ a feedback, closed-loop control scheme.

The common first step of these data-driven methods is to parse historical generation and consumption data with an offline centralized optimization algorithm that includes a representative model of the DN. This step allows to compute optimal DER setpoints for different historical operating conditions, under specific objectives, such as system losses minimization [9], [10] or reference voltage tracking [8], [11]. The solution also ensures system security and power quality by including the appropriate constraints in the optimization problem. Finally, the system uncertainties can also be taken into account [10] and the three-phase DNs can be assumed to be balanced [7]–[9], [11] or unbalanced [10], [11].

The second step uses the obtained optimal setpoints from the first step to design local DER controls for the real-time DN operation. The key idea lies on the derivation of simple and efficient optimized local controls that can mimic the behaviour of centralized optimization-based schemes without the need of any communication infrastructure.

This paper extends the authors' previous work in [8]–[13]. First, it presents and compares the state-of-the-art data-driven local control schemes based on the different local inputs they rely on. Then, it proposes an extension to an existing scheme to account for active power curtailment, and a new scheme

combining various local inputs. Finally, inspired by [14], it is the first paper, to the best of the authors' knowledge, that comments on artificial intelligence (AI) safety issues, arising from data-driven control design schemes in power systems. More specifically, the contributions of this paper are:

- An extension of the multiple-linear regression model presented in [8] to account for active power curtailment using a classification stage.
- The proposal of a hybrid scheme that combines different features of the investigated state-of-the-art data-driven control schemes.
- A comparison of existing and new methods, highlighting their strengths under normal and their behaviour under "unpredicted" operating conditions.

The remainder of the paper is organized as follows. Section II presents the mathematical formulation of the centralized BFS-OPF to obtain an AC feasible solution considering the modeling of various active measures. Section III describes some of the existing data-driven local control design schemes, while Section IV introduces the considered case study and the simulation results. Finally, conclusions are drawn in Section V.

II. STAGE I - CENTRALIZED OFFLINE OPF SCHEME

The goal of the first stage is to parse the available data that capture different operating conditions using an OPF-type scheme and derive the optimal DER setpoints. The latter are then used in Stage II to design the local controllers. It should be noted that the centralized scheme is used *offline* based on historical data gathered from low-cost monitoring devices, or typical values from literature when some parts are missing or noisy. That is, in real-time operation, we do not require monitoring and communication infrastructure.

Several centralized schemes can be used on the historical data to derive the optimal DER setpoints. Some of them use the non-convex non-linear AC power flows in an OPF framework with local solvers [4], linear approximations of the AC power flows [6] and convex relaxations [2]. Since this scheme is applied on a large number of scenarios, the computational efficiency and the feasibility guarantees with respect to the exact AC power flow model are of utmost importance.

In this work, we use an OPF framework derived from [3], [13], [15] that integrates a backward-forward sweep (BFS) [16] into the optimization problem. A high performance is achieved by exploiting the radial or weakly meshed distribution network topology, while the AC feasibility is guaranteed by performing an exact power flow calculation after each OPF iteration. The framework is briefly described below but the interested reader can find more details about a chance constrained OPF version in [17] and its three-phase extension in [10], [15]. However, it is important to reiterate that any other suitable OPF formulation for DNs can be used to derive the optimal DER setpoints.

A. OPF formulation

The objective of the operator is to guarantee a safe grid operation minimizing the system losses and its operating costs.

The cost of DER control is based on the curtailment of active energy and provision of reactive power support by DGs and the objective function is evaluated by summing the cost of DER control over all network nodes N_b , branches N_{br} and the entire time horizon N_{OPF} ,

$$\min_{\mathbf{u}} \sum_{t=1}^{N_{OPF}} \sum_{z \in \{a,b,c\}} \left\{ \sum_{j=1}^{N_b} \left(C_P \cdot P_{c,j,z,t} + C_Q \cdot Q_{ctrl,j,z,t} \right) + \sum_{i=1}^{N_{br}} C_P \cdot P_{loss,i,z,t} \right\} \cdot \Delta t \quad (1)$$

where \mathbf{u} is the vector of the available active control measures and Δt is the length of each time period. The curtailed power of the DGs connected at phase z , at node j and time t is given by $P_{c,j,z,t} = P_{g,j,z,t}^{\max} - P_{g,j,z,t}$, where $P_{g,j,z,t}^{\max}$ is the maximum available active power and $P_{g,j,z,t}$ the active power injection of the DGs. The use of reactive power support $Q_{ctrl,j,z,t} = |Q_{g,j,z,t}|$ for each DG connected to phase z of node j and time t is also minimized; $Q_{g,j,z,t}$ represents the DG reactive power injection or absorption. The coefficients C_P and C_Q represent, respectively, the DG cost of curtailing active power and providing reactive power support (DG opportunity cost or contractual agreement). We set $C_Q \ll C_P$, which prioritizes the use of reactive power control over active power curtailment. We further calculate the total losses by using the difference between input and output power in each phase [18]. Thus, $P_{loss,i,z,t} = \text{Re}(|S_{i_f,z,t} + S_{i_r,z,t}|)$, where $S_{i_f,z,t}$ and $S_{i_r,z,t}$ represent the apparent power flowing into branch i from each end; j_f and j_t are the sending and receiving ends of the branch.

The power injections at every node j , phase z and time step t are given by

$$P_{inj,j,z,t} = P_{g,j,z,t} - P_{l,j,z,t}, \quad (2a)$$

$$Q_{inj,j,z,t} = Q_{g,j,z,t} - P_{l,j,z,t} \cdot \tan(\phi_{load}), \quad (2b)$$

where $P_{l,j,z,t}$ and $P_{l,j,z,t} \cdot \tan(\phi_{load})$ are active and reactive node demands of constant power type, with $\cos(\phi_{load})$ being the power factor of the load.

A single iteration of the BFS power flow problem is considered to represent the power flow constraints. That is: $\mathbf{I}_{br,t} = \mathbf{BIBC} \cdot \left(\frac{P_{inj,j,z,t} + jQ_{inj,j,z,t}}{V_{j,z,t}^*} \right)$ and $\mathbf{V}_t = \mathbf{V}_{slack} + \mathbf{BCBV} \cdot \mathbf{I}_{br,t}$, where $V_{j,z,t}^*$ is the voltage of phase z , at node j at time t , * indicates the complex conjugate and the bar indicates that the value from the previous iteration is used (the interested reader is referred to [10] for more details); $\mathbf{I}_{br,t}$ is the vector of the three-phase branch flow currents; and, \mathbf{BIBC} (Bus Injection to Branch Current) is a matrix with ones and zeros, capturing the three-phase topology of the DN (including any single-phase laterals); $\Delta \mathbf{V}_t$ is the vector of voltage drops over all branches and phases; \mathbf{BCBV} (Branch Current to Bus Voltage) is a matrix with the complex impedance of the lines as elements (including mutual coupling); \mathbf{V}_{slack} is the three-phase voltage in per unit at the slack bus (here assumed to be $\{1 < 0^\circ, 1 < -120^\circ, 1 < 120^\circ\}$). Thus, the constraint for the current magnitude for all branches i and phase z at time t is

$$|\mathbf{I}_{br,i,t}| \leq \mathbf{I}_{i,max}, \quad (3)$$

where $\mathbf{I}_{i,max}$ is the maximum thermal limit of the three phases.

For the voltage magnitude constraint, we follow [15] and

rotate the three voltage phases $\{a, b, c\}$ by $\mathcal{R} = \{1 < 0^\circ, 1 < 120^\circ, 1 < -120^\circ\}$ to avoid the non-convex $V_{\min} \leq |V_{j,z,t}| \leq V_{\max}$ constraints yielding

$$|\mathcal{R}V_{j,z,t}| \leq V_{\max}, \quad \text{Re}\{\mathcal{R}V_{j,z,t}\} \geq V_{\min}. \quad (4)$$

Finally, the limits of the inverter-based PVs are given by

$$P_{g,j,z,t}^{\min} \leq P_{g,j,z,t} \leq P_{g,j,z,t}^{\max}, \quad (5a)$$

$$Q_{g,j,z,t}^2 \leq (S_{\text{inv},j}^{\max})^2 - P_{g,j,z,t}^2, \quad (5b)$$

where $P_{g,j,t}^{\min}$, $P_{g,j,t}^{\max}$, are the upper and lower limits for active DG power, and $S_{\text{inv},j}^{\max}$ is the j^{th} inverter's capacity.

III. STAGE II - DATA-DRIVEN LOCAL CONTROL DESIGN

In this section, we describe the mathematical models of the examined local data-driven control schemes. One key characteristic of these methods is the existence of a feedback in the control method. Open-loop schemes do not use feedback, i.e. the response of the controllers is based only on local measurements, and the output has no effect on the controller input variable. These schemes are typically stable, and simple to implement. On the contrary, in closed-loop schemes, the output of the controller has an impact on the local measurements and thus influences the controller's input through a feedback term. These schemes are generally more complex to analyze in terms of stability. However, they can be more robust in situations that are far from the ones in the training dataset.

The closed-loop schemes considered in this work use the *voltage magnitude* as a local feature to control active and reactive power results. Although voltage is a local feature, it *carries* information from the whole network due to the physics of system. Thus, we can design controllers that can perform reasonably well, even when the real-time conditions are "far" from those in the training dataset. This is important in machine learning systems to avoid *accidents*, defined in [14] as "unintended and harmful behavior that may emerge from poor design of real-world AI systems".

Another key characteristic of the different methods is the number and type of local measurements they use. They can rely only on one feature, e.g. local voltage [9], or on a set of measurements, such as local demand, generation and maximum capacities [11]. In the latter case, the set of measurements can be selected to better map the OPF setpoints into a model.

In this paper, we compare 4 methods, 2 open-loop and 2 closed-loop. In addition, we combine *the best of both worlds* by selecting and using multiple measurements following the methodology of [11], while introducing the voltage in a closed-loop manner, as in [9]. In this way, the controllers' behavior is close to the optimal and can contribute to secure operation even in unseen conditions.

For all schemes, the real-time response of the j^{th} inverter-based DER ($j \in [1, 2, \dots, N_j]$) is derived by N_{OPF} optimal setpoints ($t \in [1, 2, \dots, N_{\text{OPF}}]$) in terms of reactive power control $q_t^{(j)}$ and active power curtailment $c_t^{(j)}$ from the off-line calculations. The main goal is to derive models which will mimic the optimal setpoints using only local input measurements (features). The feature matrix $\Phi^{(j)} \in \mathbf{R}^{N_{\text{OPF}} \times N_K}$

contains as columns the N_{OPF} observations of the k^{th} input measurement $\phi_k^{(j)} \in \mathbf{R}^{N_K}$, i.e.

$$\Phi^{(j)} = \begin{bmatrix} \phi_1^{(j)} & \phi_2^{(j)} & \dots & \phi_{N_K}^{(j)} \end{bmatrix}. \quad (6)$$

For clarity reasons, we omit the subscripts of the phase z for the rest of the section.

A. Local open-loop control

1) *O1*: The first open-loop local scheme is implemented in several European countries, e.g. Germany [19]. Although it is not designed using a data-driven approach, it will be used as the *reference*. According to this scheme, the DGs have to adjust their power factor as a function of the generation.

Thus, the only feature used is active power generation $\Phi_1^{(j)} = \phi_{1,t}^{(j)} = P_{g,j,t}$. The relations giving the per unit real-time reactive power and active power curtailment are

$$\tilde{q}_t = -\tan(\text{acos}(1 - 0.1 \cdot \max(0, P_{g,j,t} - 0.5))), \quad (7a)$$

$$\tilde{c}_t = 0. \quad (7b)$$

2) *O2*: This is an extension of [8] which is based on multiple regression to account also for Active Power Curtailment (APC). However, since APC is rarely needed, i.e. only when Reactive Power Control (RPC) is not adequate to satisfy the network constraints, we propose two stages for active power curtailment: first a classification method is used to identify the requirement for curtailment, and then a regression model to predict the actual value of APC.

As base features for the reactive power control we follow [8] and use the net active power demand $\phi_{2,t}^{(j)} = P_{g,j,t} - P_{l,j,t}$, the reactive power demand $\phi_{3,t}^{(j)} = Q_{l,j,t}$, and the maximum reactive power capability of the inverter $\phi_{4,t}^{(j)} = Q_{g,j,t}^{\max}$. We also consider combinations of these features, i.e. $\phi_{5,t}^{(j)} = \phi_{2,t}^{(j)} \cdot \phi_{3,t}^{(j)}$ and $\phi_{6,t}^{(j)} = (\phi_{2,t}^{(j)})^2$. Finally, the feature matrix is given by $\Phi_2^{(j)} = [\phi_{2,t}^{(j)}, \phi_{3,t}^{(j)}, \phi_{4,t}^{(j)}, \phi_{5,t}^{(j)}]^T$. Using the least squares method, the local model for reactive power control is derived by solving

$$\min_{\alpha} \sum_{t \in N_{\text{OPF}}} (q_t^{(j)} - \tilde{q}_t^{(j)})^2, \quad (8a)$$

$$\tilde{q}_t^{(j)} = \alpha_0^{(j)} + \sum_{k \in K} \alpha_k^{(j)} \cdot \Phi_2^{(j)}, \quad (8b)$$

where $\alpha_k^{(j)}$ are the $k+1$ regression coefficients of the j^{th} unit for the $k \subset N_K$ features.

The model for the active power control consists of two steps. First, the classifier function $y_c = \text{sign}(\langle w, \Phi_3^{(j)} \rangle + b)$ that identifies if active power curtailment will be used ($y_c \in \{0, 1\}$) is found by solving the support vector machine problem

$$\min_{w,b,\xi} \frac{1}{2} w^T w + C \sum_{t=1}^{N_{\text{OPF}}} (\xi + \xi^*) \quad (9a)$$

subject to

$$y_c - \langle w, \Phi_3 \rangle - b \leq \epsilon + \xi, \forall (\Phi_3, y_c) \quad (9b)$$

$$\langle w, \Phi_3 \rangle + b - y_c \leq \epsilon + \xi^*, \forall (\Phi_3, y_c) \quad (9c)$$

$$\xi \geq 0, \xi^* \geq 0. \quad (9d)$$

where $\Phi_3^{(j)} = [\phi_{1,t}^{(j)}, \phi_{7,t}^{(j)}]^T$ is the features matrix for the classification stage with $\phi_{7,t}^{(j)} = P_{1,j,t}$; the constant C penalizes the predictions outside the region defined by ϵ , and the slack variables ξ are used to allow for prediction errors. Finally, we try different kernel functions, i.e. linear, polynomial, Gaussian, and we keep the one with the lowest overall out-of-sample error through a 5-fold cross validation process.

Similar to the reactive case, the local model for active power curtailment is derived by solving

$$\min_{\tilde{\alpha}} \sum_{t \in N_{OPF}} (c_t^{(j)} - \tilde{c}_t^{(j)})^2, \quad (10a)$$

$$\tilde{c}_t^{(j)} = \tilde{\alpha}_0^{(j)} + \sum_{k \subset K} \tilde{\alpha}_k^{(j)} \cdot \Phi_4^{(j)}. \quad (10b)$$

where $\Phi_4^{(j)} = \Phi_3^{(j)}$, and $\tilde{\alpha}_k^{(j)}$ are the $k+1$ regression coefficients of the j^{th} unit for the $k \subset N_K$ features.

B. Local closed-loop control

Inverter-based volt-var control drives voltages to desired values by establishing a relation between the measured voltage magnitude and reactive power injections. Modern grid codes allow volt-var control in distribution systems [20]. However, the same static curve is used by all inverters of similar size irrespective of their location and grid challenges. For this reason, reference [9] proposed a data driven approach to derive a different volt-var characteristic curve for each inverter, based on its location and the system-wide challenges.

1) *C1*: Following [10], we use segmented-regression to derive APC and RPC piece-wise linear curves, optimizing also the placement of the break-points. These curves are similar to the ones used today in industry and grid codes. However, in contrast to existing standards, the proposed characteristic curves might have an arbitrarily large number of piece-wise linear segments and are optimized for each individual DG, based on the location of the DGs and the DN challenges.

Obtaining the optimal break-points and the slope coefficients is a non-linear and non-differentiable problem. Thus, following [10] and inspired by [21], we iteratively derive the location of the break-points while solving a residual sum-of-squares (RSS) optimization problem for the slope coefficients. The procedure is summarized below and interested readers are referred to [10] for further details.

First, we define the number of break-points n_s ($\bar{k} \in \{1, 2, \dots, n_s\}$), initialize them, and solve the residual sum of squares problem

$$RSS_{\bar{i}} := \min_{\tilde{x}_0, \beta, s, \gamma} \sum_{t \in N_{OPF}} P_{g,j,t} \cdot (x_t - \tilde{x}_t)^2 + \sum_{\bar{k}=1}^{n_s} \gamma_{\bar{k}}^2$$

subject to

$$\tilde{x}_t = \tilde{x}_0 + \beta_0 \cdot \Phi_5^{(j)} + \sum_{\bar{k}=1}^{n_s} \beta_{\bar{k}} \cdot (\Phi_5^{(j)} - s_{\bar{k}}^j) \cdot I(\Phi_5^{(j)} > s_{\bar{k}}^j) - \sum_{\bar{k}=1}^{n_s} \gamma_{\bar{k}} \cdot I(\Phi_5^{(j)} > s_{\bar{k}}^j)$$

Monotonicity and slope constraints.

As input we use the voltage vector $\phi_{8,t}^{(j)} = [|V_{j,t}|]$ with $\Phi_5^{(j)} = [\phi_{8,t}^{(j)}]$. We fit the linear model based on the known breakpoints $s_{\bar{k}}^j$, $\forall \bar{k} = 1, \dots, n_s$ at the current iteration \bar{i} , the left slope β_0 and difference-in-slopes $\beta_{\bar{k}}$. The indicator function $I(\cdot)$

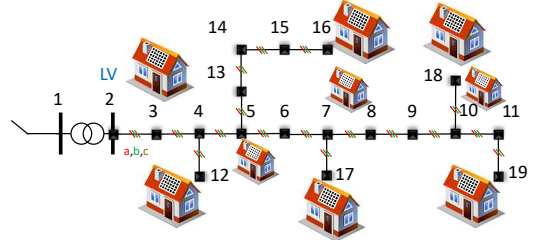


Fig. 1. Cigre LV grid.

becomes one when the inside statement is true. Finally, \tilde{x}_0 is the model intercept and γ a parameter which updates the location of the breakpoints towards the optimal one. Then, we update the breakpoints $s_{\bar{k}}^{\bar{i}+1} = \frac{\gamma_{\bar{k}}}{\beta_{\bar{k}}} + s_{\bar{k}}^{\bar{i}}$ and iteration index $\bar{i} = \bar{i} + 1$, repeating the procedure until the RSS does not change between two iterations.

The same method is used both for the APC and RPC curves, using respectively the PV optimal active and reactive setpoints from the OPF in Section II.

2) *C2*: This scheme extends the model presented in Section III-A2 to account also for local voltages, resulting in a feedback control scheme. More specifically, the updated feature matrices are $\Phi_6^{(j)} = [\Phi_2^{(j)}, \phi_{8,t}^{(j)}]^T$, $\Phi_7^{(j)} = [\Phi_3^{(j)}, \phi_{8,t}^{(j)}]^T$ and $\Phi_8^{(j)} = [\Phi_4^{(j)}, \phi_{8,t}^{(j)}]^T$ and are used in (8), (9) and (10) to derive the regression coefficients for this dynamic control scheme.

IV. CASE STUDY - RESULTS

A. Network description - Case study setup

To demonstrate the performance of the four methods, we use the benchmark radial residential LV grid presented in [22] and shown in Fig. 1. The load and PV panels are distributed to the three phases unevenly, resulting in unbalanced conditions. The total load, taken from [22], is shared 25%-60%-15% among the three phases. The installed PV capacity, is set to $S_{\text{rated}}^{\text{PV}} = 150\%$ of the total maximum load of the entire feeder to the PV nodes = [3, 5, 7, 10, 12, 16, 17, 18, 19], and is shared 25%-25%-50% among the three phases.

In the design stage, we use the algorithm in Section II to process a 30-day summer dataset with forecasts of load and PV production, and generate the optimal DER setpoints. The operational costs of the centralized problem are assumed to be $c_P = 0.3 \frac{\text{CHF}}{\text{kWh}}$ and $c_Q = 0.01 \cdot c_P$. From the optimal DER data, we derive the three data-driven schemes (O1, C1, C2) as described in Section III. Then, we evaluate their performance, and compare it to O1 and the optimal (OPF-based), using data from another summer month. The implementation was done in MATLAB using YALMIP [23] as the modeling layer and Gurobi [24] as the solver. The results were obtained on an Intel Core i7-2600 CPU and 16 GB of RAM.

B. Derived local control schemes

1) Local open-loop control:

a) *O1*: Fig. 2 shows the $\cos\phi = f(P)$ characteristic curve defined in [19]. Larger units require more reactive power absorption when the DG injects above 0.5 p.u.

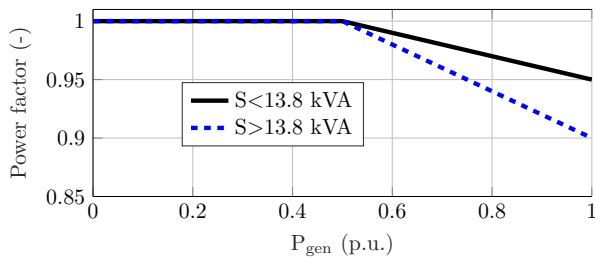


Fig. 2. Open-loop power factor adjustment.

b) *O2*: Figure 3 shows the boundaries for APC activation. As it is expected, PV generation above a certain threshold, i.e. $\phi_1^{19} \approx 0.8$ p.u. in this case, would lead to power quality issues, e.g. overvoltages or thermal overloads. However, at high (low) levels of local load (ϕ_7^{19}), the boundary threshold value increases (decreases), since more (less) active power can be consumed by the local load.

2) Local closed-loop control:

a) *C1*: Figure 4 presents the local volt-var characteristic curves derived according to Section III-B1 of all PV units in phase C. Node 3 injects reactive power to optimize losses, while the remaining nodes absorb reactive power at voltages smaller than the maximum acceptable value of 1.04 p.u..

b) *C2*: As described in Section III-A2, regression models are calculated for each DER unit using the feature-matrix Φ_2 for the open-loop *O2* and Φ_6 for the closed-loop *C2* scheme, respectively. Table I shows the dominant features for both cases, for all phases at Node 3 (close to the substation) and at Node 19 (at the end of the feeder). In contrast to [11], here the behavior of the DERs is based mostly on the inverter maximum capacity (ϕ_4). Phases *a* and *b* do not face overvoltage or overloading challenges, and thus, they show a capacitive behavior injecting reactive power to optimize losses. On the other hand, Phase *c*, hosting the biggest share of PV units, shows inductive behavior at hours with high solar radiation to reduce voltages.

C. Method Comparison

In this section, we investigate the ability of open- and closed-loop local schemes to emulate the centralized behavior. First, we consider operating conditions similar to the training dataset. Second, we explore the robustness of the schemes

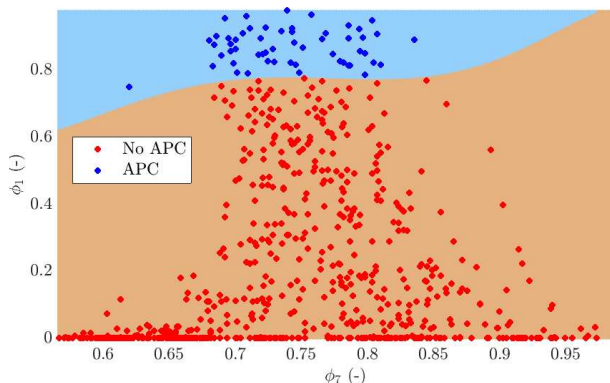


Fig. 3. Active power curtailment (APC) classification regions for the real-time response of the DER based on local load and PV generation.

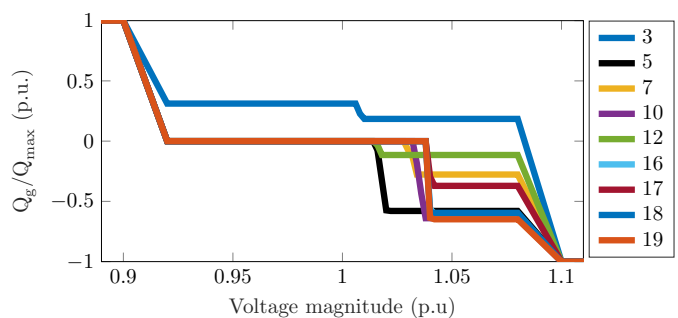


Fig. 4. Individual local characteristic curves for reactive power control of the PV units at phase C.

TABLE I
NORMALIZED COEFFICIENT OF THE DOMINANT FEATURE AT NODE 19.

	Dominant Feature			
	O2		C2	
	Node 3	Node 19	Node 3	Node 19
Phase a	ϕ_4	ϕ_2	ϕ_4	ϕ_8
Phase b	ϕ_4	ϕ_2	ϕ_4	ϕ_4
Phase c	ϕ_2	ϕ_4	ϕ_4	ϕ_4

when the given inputs are significantly different from the training sets, providing some insights on a safety issue of AI-based control methods.

1) *Expected operating conditions*: Table II summarizes the results in terms of losses, highest voltage and thermal loading, and the needed active power curtailment from applying all methods in real-time operation for a period of one summer month (different from the one used in the training stage). As can be seen, the OPF satisfies all security constraints. Method *O1* (standard industry practice) results in higher maximum loading due to increased needs for reactive power by the PV units, without solving the overvoltage issue. Methods *O2*, *C1* and *C2* mitigate adequately the power quality issues with marginal violations which are acceptable by grid codes, while being capable of mimicking satisfactorily the OPF-based control without the need of communication. This can be seen also in Fig. 5 that shows the voltage magnitude evolution of Node 19, the worst in terms of maximum voltage node.

2) *Robustness to different conditions*: Here we use the same seasonal characteristics, but the network has changed by installing a new PV unit, or connecting an additional load. These conditions were not seen in the training data, and the focus here is to assess how the controllers will behave under an unseen setup without re-training. In order to examine the

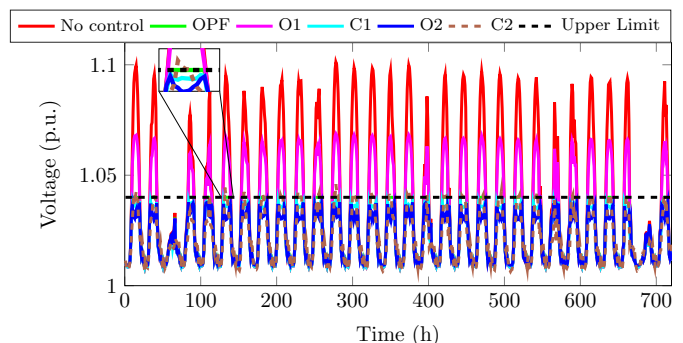


Fig. 5. Monthly voltage magnitude evolution at Node 19, phase C.

TABLE II
SUMMARIZED MONTHLY RESULTS FOR ALL METHODS (ONLY THE
LARGEST OBSERVED VALUE IS LISTED)

Method	No control	OPF	O1	C1	O2	C2
Losses (%)	4.19	4.82	4.602	3.722	4.475	4.812
$ V _{\max}$ (p.u.)	1.09	1.04	1.069	1.039	1.038	1.042
$ I _{\max}$ (%)	112	100	119.9	91.5	104.2	101.5
P_c (%)	0	0.96	0	4.93	1.16	1.18

locational impact, we consider two locations for these changes; that is, at Node 4 - close to the secondary of the transformer, and at Node 11 - almost at the end of the feeder, both at phase C. The added PV unit and load are chosen as 50% of the respective values of PV capacity and load of Node 19.

Figure 6 shows the boxplots (minimum, first quartile, median, third quartile, and maximum values) for the monthly voltage magnitude at Phase C of Node 19, for all methods. In all cases, adding a PV unit at Node 11 (away from the substation) results in higher grid voltages, compared to Node 4 which is close to the transformer where voltage is regulated. As with the previous tests, method O1 is the most inefficient, imposing a certain behavior to all DGs. Methods C1, O2 and C2 behave satisfactorily, with overvoltages only when adding a PV at Node 11. In this case, Method C2 achieves the best performance since it reacts to the measured voltage, although the change has occurred elsewhere in the grid. This highlights the benefit of method C2, since voltage inherently brings global information through the physics of the system. Finally, the two load cases are similar, because the amount of load that is added is relative low and does not influence the voltages significantly.

V. CONCLUSION

In the future, active DNs will rely on controlling DERs to ensure a safe, reliable and optimal operation of the grid. On the one hand, centralized, OPF-based controllers achieve optimal results, but rely on communication and monitoring infrastructure. On the other hand, local schemes are robust and inexpensive, but cannot cope efficiently with the modern challenges of DNs. In this paper, we examine data-driven local control schemes, trained off-line to mimic the centralized optimal behavior without the need for monitoring and communication infrastructure. We revisited existing methods, proposed a new variation (C2), and compared in terms of performance under normal and unseen conditions. Future work

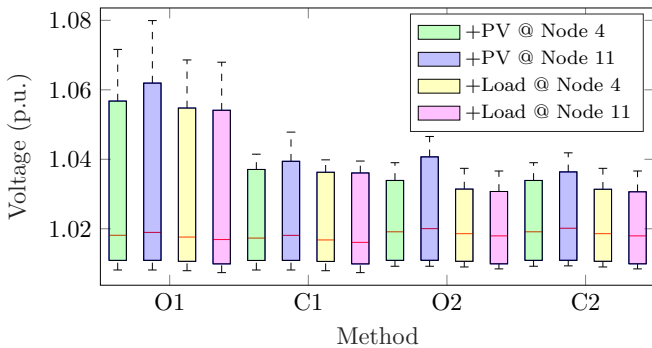


Fig. 6. Boxplots of the voltage magnitudes for all methods when a new PV unit or load is installed at Node 19, phase C.

will focus on the inclusion of safety constraints in the design stage of such controllers.

REFERENCES

- [1] N. Hatziaargyriou, O. Vlachokyriakou, T. Van Cutsem, J. Milanović, P. Pourbeik, C. Vournas, M. Hong, R. Ramos, J. Boemer, P. Aristidou, V. Singhvi, J. dos Santos, and L. Colombari, "IEEE PES Task Force on Contribution to Bulk System Control and Stability by Distributed Energy Resources connected at Distribution Network," Tech. Rep., 2017.
- [2] J. Lavaei and S. H. Low, "Zero duality gap in optimal power flow problem," *IEEE Trans. on Power Systems*, vol. 27, no. 1, pp. 92–107, 2012.
- [3] P. Fortenbacher, M. Zellner, and G. Andersson, "Optimal sizing and placement of distributed storage in low voltage networks," in *Proc. of the 19th PSCC, Genova*, Jun 2016.
- [4] S. Karagiannopoulos, P. Aristidou, A. Ulbig, S. Koch, and G. Hug, "Optimal planning of distribution grids considering active power curtailment and reactive power control," *IEEE PES General Meeting*, 2016.
- [5] P. Kotsampopoulos, N. Hatziaargyriou, B. Bletterie, and G. Lauss, "Review, analysis and recommendations on recent guidelines for the provision of ancillary services by Distributed Generation," in *IEEE International Workshop on Intelligent Energy Systems, IWIES*, 2013.
- [6] S. Bolognani and S. Zampieri, "A distributed control strategy for reactive power compensation in smart microgrids," *IEEE Transactions on Automatic Control*, vol. 58, no. 11, pp. 2818–2833, Nov. 2013.
- [7] A. Garg, M. Jalali, V. Kekatos, and N. Gatsis, "Kernel-Based Learning for Smart Inverter Control," 2018. [Online]. Available: <http://arxiv.org/abs/1807.03769>
- [8] O. Sondermeijer, R. Dobbe, D. Arnold, and C. Tomlin, "Regression-based Inverter Control for Decentralized Optimal Power Flow and Voltage Regulation," *IEEE PES General Meeting*, 2016.
- [9] S. Karagiannopoulos, P. Aristidou, and G. Hug, "Hybrid approach for planning and operating active distribution grids," *IET Generation, Transmission & Distribution*, pp. 685–695, Feb 2017.
- [10] S. Karagiannopoulos, P. Aristidou, and G. Hug, "Data-driven Local Control Design for Active Distribution Grids using off-line Optimal Power Flow and Machine Learning Techniques," *Accepted in IEEE Transactions on Smart Grid*, 2019, doi: 10.1109/TSG.2019.2905348.
- [11] R. Dobbe, O. Sondermeijer, D. Fridovich-Keil, D. Arnold, D. Callaway, and C. Tomlin, "Data-Driven Decentralized Optimal Power Flow," 2018. [Online]. Available: <http://arxiv.org/abs/1806.06790>
- [12] F. Bellizio, S. Karagiannopoulos, P. Aristidou, and G. Hug, "Optimized local control schemes for active distribution grids using machine learning techniques," in *IEEE PES General Meeting 2018*, June 2018.
- [13] S. Karagiannopoulos, P. Aristidou, and G. Hug, "Co-optimisation of Planning and Operation for Active Distribution Grids," in *Proc. of the 12th IEEE PES PowerTech, Manchester*, Jun 2017.
- [14] D. Amodei, C. Olah, J. Steinhardt, P. Christiano, J. Schulman, and D. Mané, "Concrete Problems in AI Safety," 2016. [Online]. Available: <http://arxiv.org/abs/1606.06565>
- [15] S. Karagiannopoulos, P. Aristidou, and G. Hug, "A Centralised Control Method for Tackling Unbalances in Active Distribution Grids," in *Proc. of the 20th PSCC, Dublin*, June 2018.
- [16] J. H. Teng, "A direct approach for distribution system load flow solutions," *IEEE Trans. on Power Delivery*, vol. 18, pp. 882–887, 2003.
- [17] S. Karagiannopoulos, P. Aristidou, L. Roald, and G. Hug, "Operational Planning of Active Distribution Grids under Uncertainty," in *IREP 2017, X Bulk Power Systems Dynamics and Control Symposium*, Aug 2017.
- [18] W. H. Kersting, *Distribution System Modeling and Analysis*, 2002.
- [19] VDE-AR-N 4105, "Power generation systems connected to the LV distribution network." FNN, Tech. Rep., 2011.
- [20] IEEE 1547, "IEEE Standard for Interconnecting Distributed Resources with Electric Power Systems," Jul 2003.
- [21] V. M. R. Muggeo, "Estimating regression models with unknown breakpoints," *Statistics in Medicine*, vol. 22, no. 19, pp. 3055–3071, Oct 2003.
- [22] K. Strunz, E. Abbasi, C. Abbey, C. Andrieu, F. Gao, T. Gaunt, A. Gole, N. Hatziaargyriou, and R. Iravani, "Benchmark Systems for Network Integration of Renewable and Distributed Energy Resources," *CIGRE, Task Force C6.04*, no. 273, pp. 4–6, 4 2014.
- [23] J. Löfberg, "Yalmip: A toolbox for modeling and optimization in matlab," in *Proc. of the CACSD Conference*, Taiwan, 2004.
- [24] I. Gurobi Optimization, "Gurobi optimizer reference manual," 2016. [Online]. Available: <http://www.gurobi.com>